Electronic Supplementary Information

for

A new family of Fe_2Ln complexes built from mononuclear anionic Schiff base subunits

Ivan Nemec,[a] Marek Machata,[a] Radovan Herchel,[a] Roman Boča,[b] and Zdeněk Trávníček[a*]

[a] *Regional Centre of Advanced Technologies and Materials, Department of Inorganic Chemistry, Faculty of Science, Palacký University, Tř. 17. Listopadu 12, CZ-77146 Olomouc, Czech Republic.*
[b]*Institute of Inorganic Chemistry, Slovak University of Technology, Radlinského 9, SK-812 37, Bratislava, Slovakia.*

CONTENT

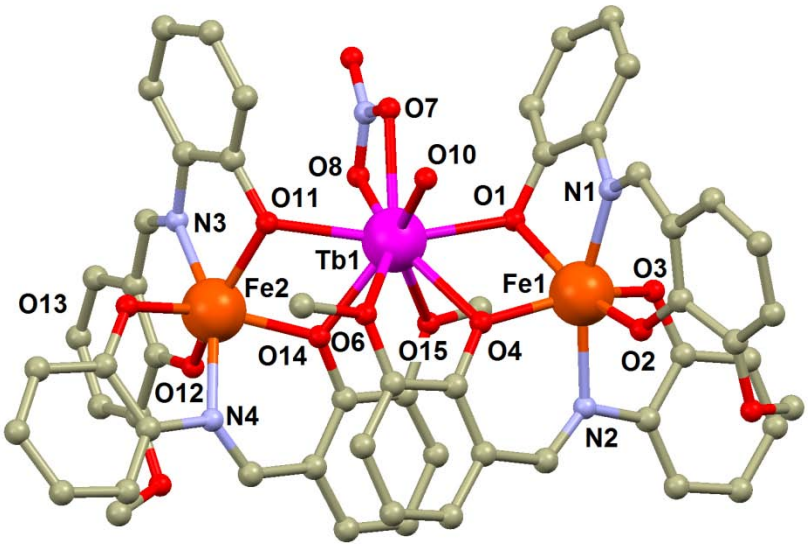

Fig. S1 The molecular structure of $[\{Fe(3MeO\text{-}L)_2\}_2Tb(NO_3)(H_2O)]$ **2b**. H-atoms were omitted for clarity. Selected bond lengths (in Å): N1-Fe1 = 2.135(3), N2-Fe1 = 2.184(3), N4-Fe2 = 2.215(3), N3-Fe2 = 2.130(3), O1-Fe1 = 2.099(2), O1-Tb1 = 2.350(2), O2-Fe1 = 1.939(3), O3-Fe1 = 1.950(3), O4-Fe1 = 2.008(2), O4-Tb1 = 2.345(2), O6-Tb1 = 2.673(2), O7-Tb1 = 2.440(3), O8-Tb1 = 2.464(2), O10-Tb1 = 2.344(2), O11-Fe2 = 2.068(2), O11-Tb1 = 2.379(2), O12-Fe2 = 1.928(2), O13-Fe2 = 1.937(2), O14-Fe2 = 1.998(2), O14-Tb1 = 2.321(2), O15-Tb1 = 2.658(2)

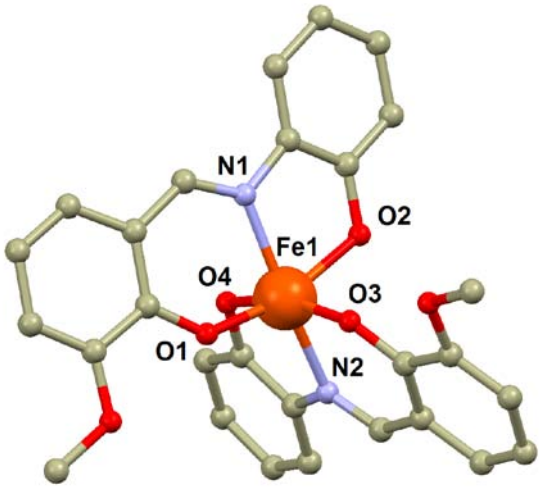

Fig. S2 The molecular structure of the $[Fe(3MeO\text{-}L)_2]^-$ anion. H-atoms were omitted for clarity. Selected bond lengths (in Å): N1-Fe1 = 2.139(2), N2-Fe1 = 2.148(2), O1-Fe1 = 1.954(2), O2-Fe1 = 2.016(2), O3-Fe1 = 1.941(2), O4-Fe1 = 1.988(2)

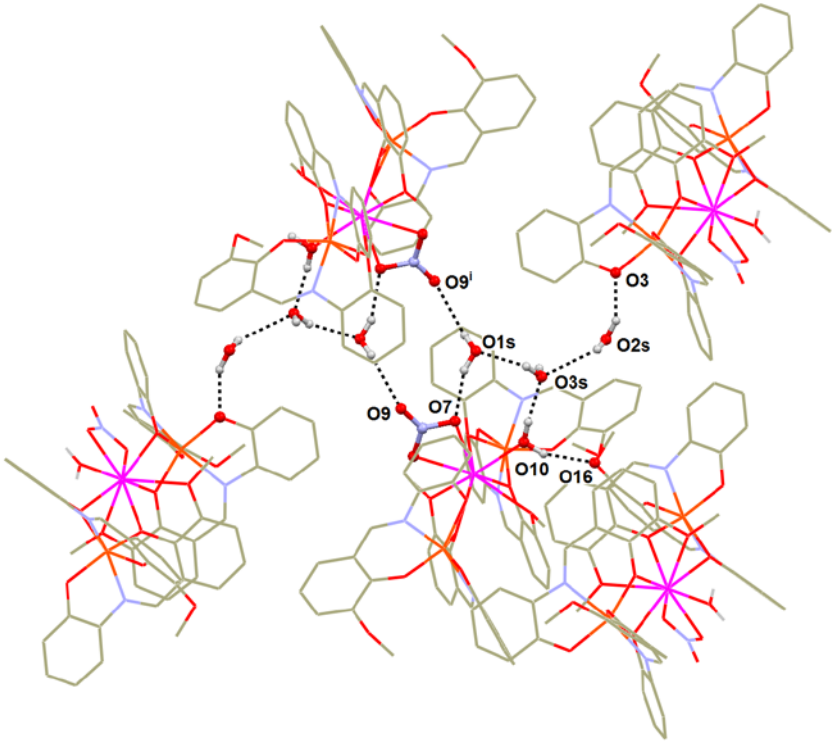

Fig. S3 A perspective view on the hydrogen bonding in the crystal structure of **2b**. Selected parameters of the non-covalent contacts (the donor-acceptor distances in Å): d(O1s…O7) = 2.906(4), d(O1s…O9) = 3.106(5), *d*(O3s…O1s) = 2.783 (5), *d*(O2s…O3) = 2.754 (5), *d*(O2S…O3S) = 3.054 (7), *d*(O10…O3s) = 2.652 (4), *d*(O10…O16) = 2.801 (3)

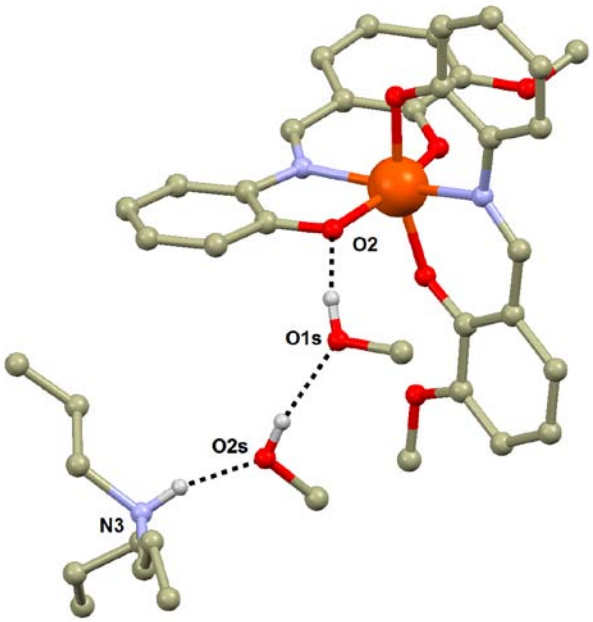

Fig. S4 A perspective view on the hydrogen bonding in the crystal structure of **1**. Selected parameters of the non-covalent contacts (the donor-acceptor distances in Å):d(N3…O2s) = 2.671(12), d(O2s…O1s) = 2.832 (6), d(O1s…O2) = 2.740 (5)

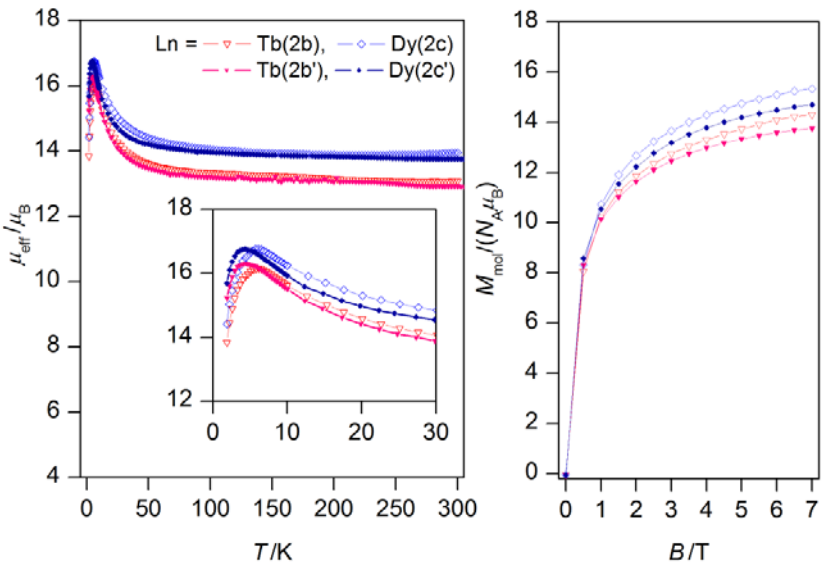

Fig. S5 Comparison of magnetic properties for **2b** vs. **2b‘** and **2c** vs. **2c‘**. *Left*: temperature dependence of the effective magnetic moment (calculated from magnetization at B = 0.1 T), with the low-temperature region expanded in the inset. *Right*: field dependence of magnetization at T = 2 K.

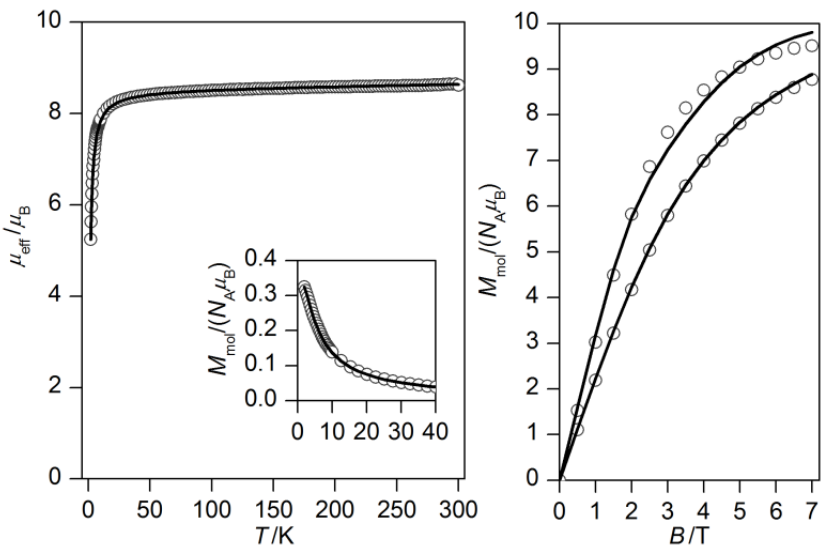

Fig. S6 Magnetic properties of **2f**. *Left*: temperature dependence of the effective magnetic moment (calculated from magnetization at B = 0.1 T), with the low-temperature region expanded in the inset. *Right*: field dependence of magnetization at T = 2 and 5 K. Circles – experimental points, lines – calculated using the best-fit parameters J_{FeFe} = -0.09 cm^{-1}, g = 2.04, D_{Fe} = −0.98 cm^{-1}, zj = -0.16 cm^{-1} and χ_{TIP} = 11.6×10^{-9} m^{3}mol^{-1}.

Magnetic data of monomeric $(Prp_3NH)[Fe(L)_2].2CH_3OH$ **(1)** were analyzed using the spin Hamiltonian:

$$\hat{H} = D(\hat{S}_{i,z}^2 - \hat{S}_i^2 / 3) + \mu_B B g \hat{S}_a$$

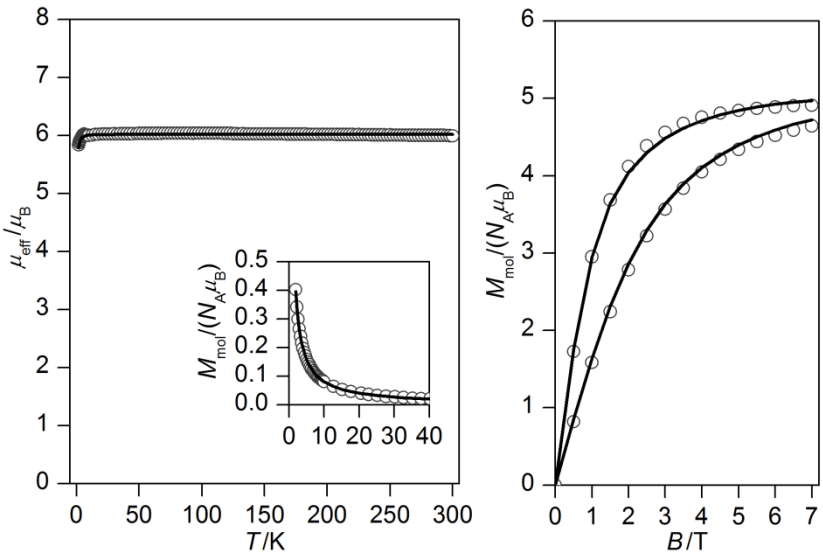

Fig. S7 Magnetic properties of **1**. *Left*: temperature dependence of the effective magnetic moment (calculated from magnetization at B = 0.1 T), with the low-temperature region expanded in the inset. *Right*: field dependence of magnetization at T = 2 and 4.6 K. Circles – experimental points, lines – calculated using the best-fit parameters g = 2.03, D = +0.80 cm^{-1}.

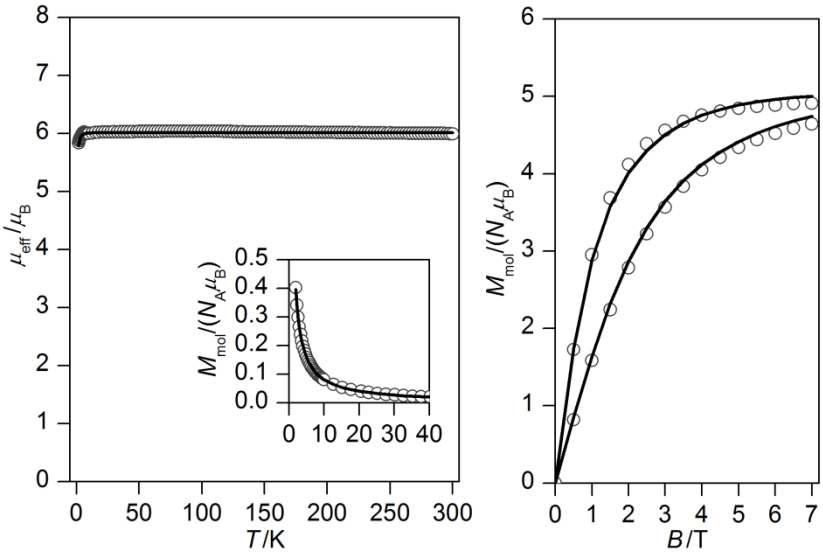

Fig. S8 Magnetic properties of **1**. *Left*: temperature dependence of the effective magnetic moment (calculated from magnetization at B = 0.1 T), with the low-temperature region expanded in the inset. *Right*: field dependence of magnetization at T = 2 and 4.6 K. Circles – experimental points, lines – calculated using the best-fit parameters g = 2.03, D = –0.64 cm^{-1}.

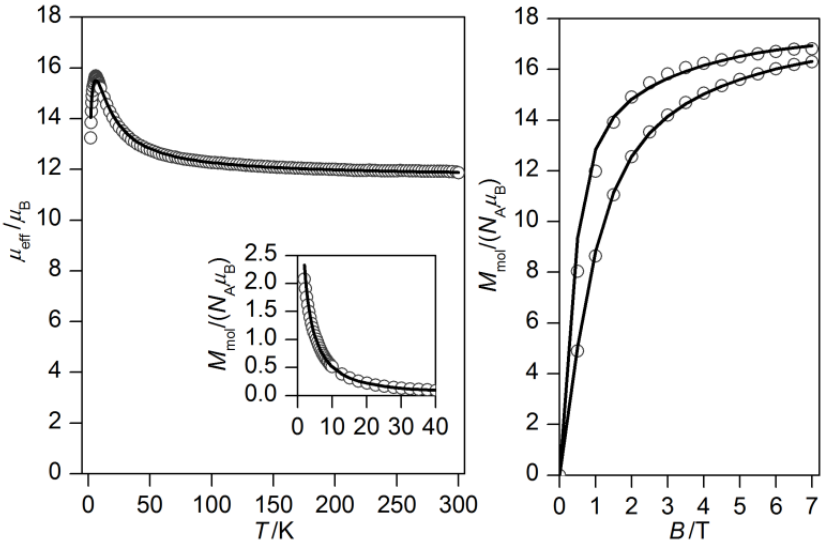

Fig. S9 Magnetic properties of **2a**. *Left*: temperature dependence of the effective magnetic moment (calculated from magnetization at B = 0.1 T), with the low-temperature region expanded in the inset. *Right*: field dependence of magnetization at T = 2 and 5 K. Circles – experimental points, lines – calculated using the best-fit parameters J_{GdFe} = +1.37 cm^{-1}, g = 2.02, D_{Gd} = +1.57 cm^{-1} and zj = -0.027 cm^{-1} with fixed J_{FeFe} = -0.09 cm^{-1} and D_{Fe} = −0.98 cm^{-1}.

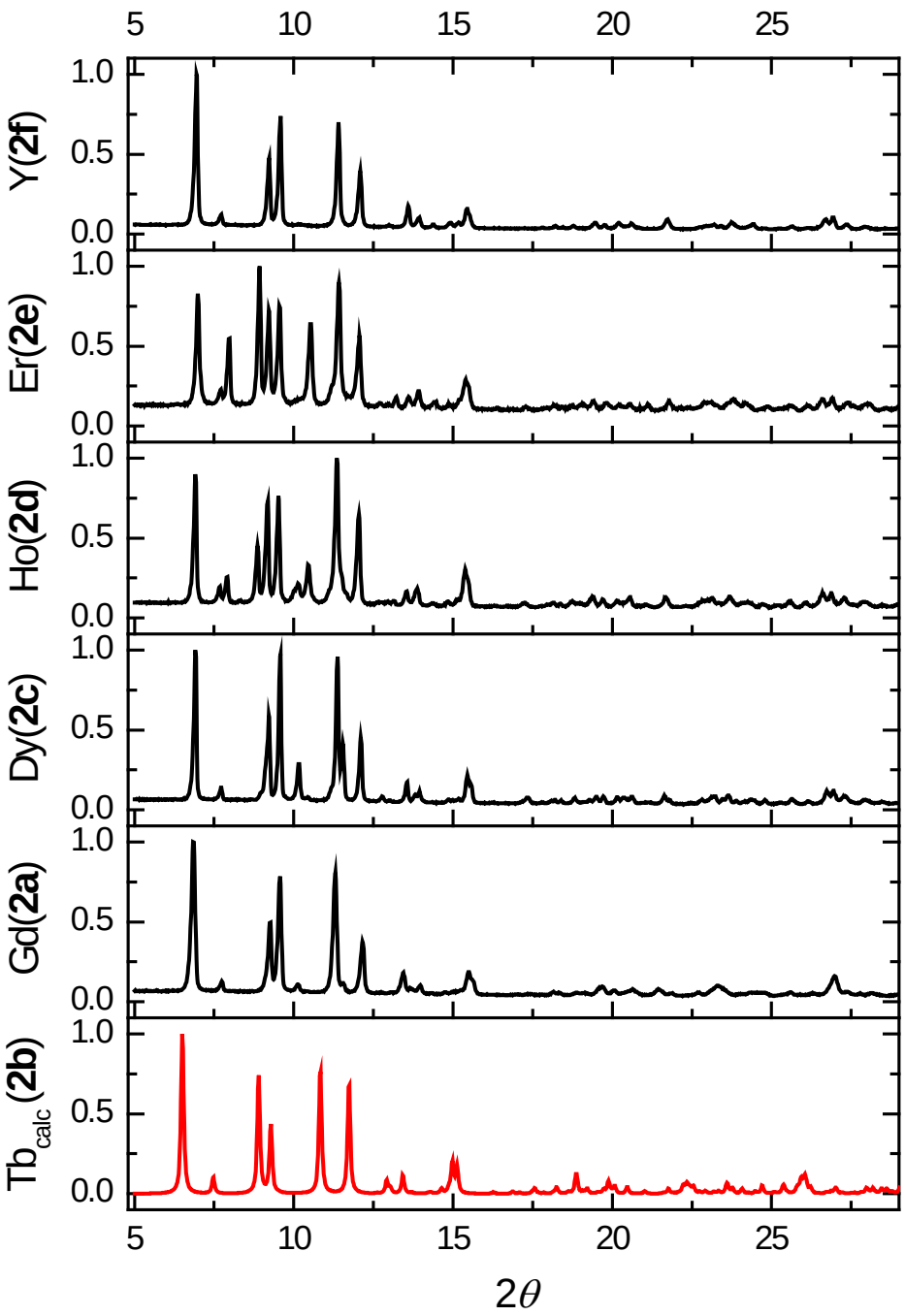

Fig. S10 Powder diffraction patterns of the trinuclear **2a-f** compounds. The powder diffraction pattern of **2b** was calculated from the single-crystal data (red line). All the patterns were compared visually with calculated one and it is apparent that the crystal structures of the **2a-f** compounds are, in main, very similar.

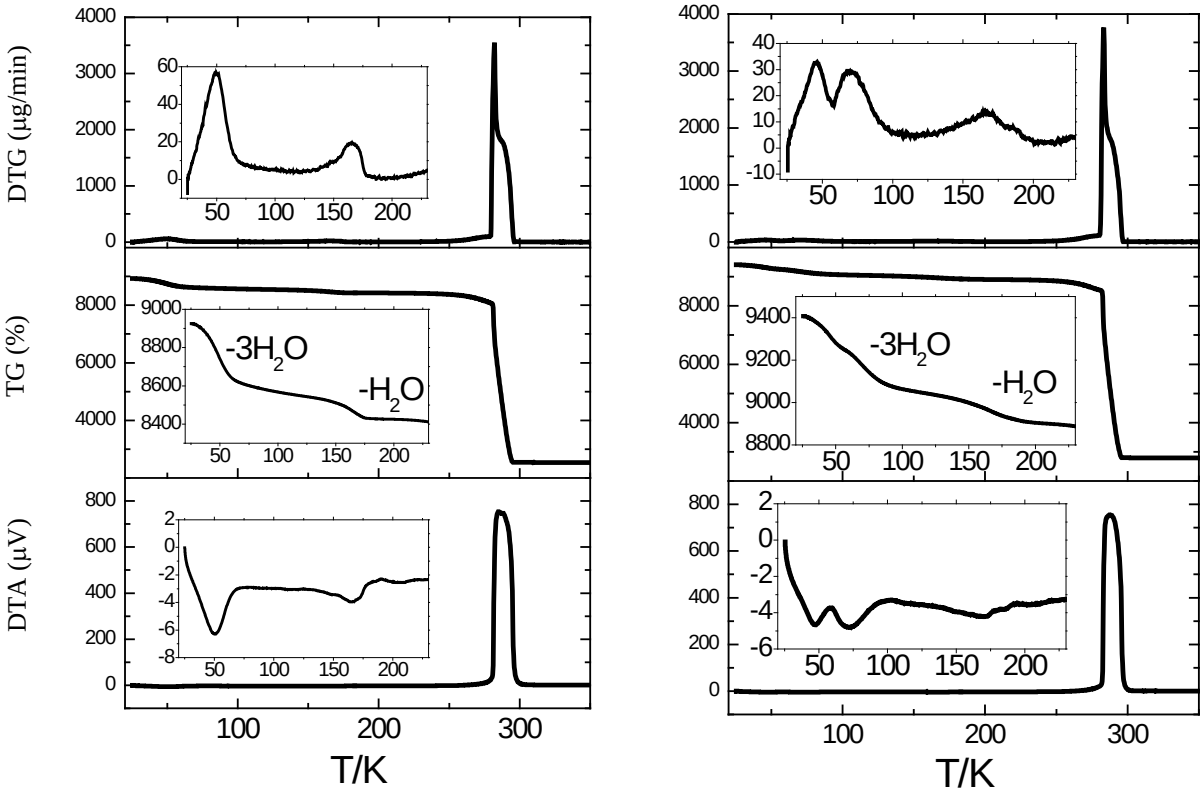

Fig. S11 Thermogravimetric data for the Fe_2Tb (**2b**) and Fe_2Dy (**2c**) compounds. The dehydration proceeds in two distinct steps.